Journal of Integrative Agriculture 2026, 25(2): 648–658

Available online at ScienceDirect

Journal of Integrative Agriculture



RESEARCH ARTICLE

Delayed photosynthesis response causes carbon assimilation reduction in soybean under fluctuating light

Jing Gao*, Shenglan Li*, Yi Lei, Qi Wang, Zili Ning, Zhaohong Lu, Xianming Tan, Mei Xu, Feng Yang#, Wenyu Yang

College of Agronomy, Sichuan Agricultural University/Sichuan Engineering Research Center for Crop Strip Intercropping System/Key Laboratory of Crop Ecophysiology and Farming System in Southwest, Ministry of Agriculture and Rural Affairs, Chengdu 611130, China

Highlights

- Soybeans grown under conditions of fluctuating light exhibit characteristics reminiscent of those adapted to low-light, including decreases in dry matter mass, leaf thinning, specific leaf weight, and chlorophyll (Chl) *a*/Chl *b* levels.
- The inhibitory impact of fluctuating light conditions on the growth of soybean plants arises from a decrease in carbon assimilation. However, this is not attributed to acclimation to low-light periods, as the photosynthetic capacity remains unaffected by fluctuating light.
- The decrease in carbon assimilation is ascribed to a delayed photosynthetic response to fluctuations in light intensity. When transitioning from low- to high-light, the gradual rate of stomatal opening limits carbon supply. Moreover, upon returning to low-light, the gradual relaxation of photoprotection hinders light utilization efficiency.

Abstract

Plants encounter dynamic light environments in natural field conditions, and species differ in their physiological and biochemical mechanisms for acclimating to fluctuating light (FL). The manner in which soybean (*Glycine max* (L.) Merr.) coordinates multiple physiological adjustments to FL remains poorly understood. This study assessed the effects of FL on soybean morphology and photosynthetic traits by examining changes in photosynthetic gas exchange parameters and chlorophyll (Chl) *a* fluorescence under alternating high- and low-light conditions. Results indicated that soybeans exposed to FL exhibited reduced dry matter accumulation, smaller and thinner leaves, and a lower Chl *a*/Chl *b* levels — characteristics typically associated with plants grown under continuous low-light. Despite these morphological similarities, their photosynthetic gas exchange rates and photosynthetic capacity were maintained at levels comparable to those under steady high light, unlike plants grown under constant low-light. Thus, acclimation to FL is distinct from adaptation to sustained low-light conditions. Correlation analyses revealed that the decline in carbon assimilation under FL primarily stemmed from two factors: the slow recovery of stomatal conductance upon transition to high light and the delayed relaxation of nonphotochemical quenching when light intensity decreased. Therefore, the reduction in carbon assimilation under FL cannot be attributed to low-light phase adjustments but rather reflects a lag in photosynthetic responsiveness to changing light conditions.

Keywords: soybean, fluctuating light, CO_2 assimilation, dynamic photosynthesis, photosynthetic limitation, stomatal opening, non-photochemical quenching

1. Introduction

Light is essential for plant photosynthesis, yet it constitutes a highly heterogeneous resource in nature, with intensity varying significantly across time and space (Yao *et al.* 2017; Huber *et al.* 2021). Within crop canopies, the actual light environment arises from a combination of environmental

Received 11 March 2024; Received in revised form 31 May 2024; Accepted 18 June 2024; Available online 22 July 2024
Jing Gao, E-mail: 2020201020@stu.sicau.edu.cn; Shenglan Li, E-mail: lishenglan@stu.sicau.edu.cn; #Correspondence Feng Yang, E-mail: f.yang@sicau.edu.cn
* These authors contributed equally to this study.

© 2026 CAAS. Publishing services by Elsevier B.V. on behalf of KeAi Communications Co. Ltd. This is an open access article under the CC BY-NC-ND license (http://creativecommons.org/licenses/by-nc-nd/4.0/). Peer review under responsibility of Editorial Board of *Journal of Integrative Agriculture*.
doi: 10.1016/j.jia.2024.07.032

conditions and cultivation practices. Intercropping and close planting are key strategies to enhance crop acreage and yield (Wu Y *et al.* 2023; Zheng *et al.* 2023). However, these practices often lead to a rapid decline in individual plant biomass due to intensified mutual shading, which reduces leaf light availability and causes frequent fluctuations in irradiance (Pignon *et al.* 2017; Wu H Y *et al.* 2023). Research indicates that experiments conducted under constant light may not accurately reflect field conditions (Matsubara 2018).

As sessile organisms, crops must acclimate to dynamic environmental conditions. One approach to increasing food production involves improving photosynthetic efficiency under natural fluctuating light (FL) conditions. Achieving such improvements requires a deeper understanding of the mechanisms underlying crop responses to FL. Pao *et al.* (2019) found that cucumber leaves grown under FL exhibit lower photosynthetic parameters than those grown under constant light. When *Arabidopsis thaliana* was cultivated under FL, reductions in biomass, leaf thickness, and photosynthetic capacity were observed (Vialet-Chabrand *et al.* 2017; Matthews *et al.* 2018). The maximum net photosynthetic rate (A_{sat}) increased significantly in petunia and tomato under FL, but no significant difference was detected in chrysanthemum (Blom and Zheng 2009). Moreover, variations in the frequency of light fluctuations had minimal impact on total plant biomass and photosynthetic capacity in tomato (Zhang *et al.* 2020).

The level of plant carbon assimilation under FL depends on both photosynthetic capacity and dynamic photosynthetic efficiency. When a leaf adapted to low-light (LL) transitions from shade to full sunlight, a delay of several minutes occurs before maximum photosynthetic rates are achieved (Yamori *et al.* 2020). This induction lag can negatively affect daily carbon gain through photosynthesis. In wheat, up to 21% of potential carbon assimilation may be lost in a single day due to delayed photosynthetic induction (Taylor and Long 2017). Electron transport responds rapidly, whereas stomatal conductance takes 30–60 min to reach its maximum, exceeding the 5–10 min required for activation of Calvin cycle enzymes such as Rubisco (Mcausland *et al.* 2016). The dynamic regulation of stomatal conductance under FL has been highlighted as critical. Mutants including slow anion channel-associated 1 (*slac1*), open stomata 1 (*ost1*), and abscisic acid-deficient *flacca* exhibit faster stomatal opening and show enhanced photosynthetic rates under FL (Kaiser *et al.* 2020; Kimura *et al.* 2020; Yamori *et al.* 2020).

Non-photochemical quenching (NPQ) is another key factor limiting photosynthetic efficiency under FL. During high-light (HL) periods, leaves dissipate excess absorbed energy efficiently *via* NPQ (Bassi and Dall'Osto 2021). However, the relaxation of NPQ lags during transitions to LL, causing a transient reduction in the quantum yield of CO_2 fixation (Wang *et al.* 2020). Kromdijk *et al.* (2016) used bioengineering to accelerate NPQ relaxation, resulting in improved electron transport efficiency in PSII and increased shoot biomass in tobacco under FL. Conversely, accelerated relaxation from photoprotection reduced photosynthetic rate and growth in transgenic potato (Lehretz *et al.* 2022). Similarly, transgenic *Arabidopsis* lines showed no biomass enhancement due to compromised photoprotection from faster NPQ relaxation (Garcia-Molina and Leister 2020).

In summary, physiological and biochemical responses to FL vary among species. The effects of FL on photosynthetic carbon assimilation in many crops, including soybean, remain poorly understood. Soybean is a major crop valued for its protein and oil content. Among 37 soybean genotypes, photosynthetic capacities do not differ significantly, but the speed of photosynthetic induction varies widely (Soleh *et al.* 2017), indicating substantial potential for optimizing photosynthesis under FL. We simulated natural light fluctuations under controlled conditions to better understand plant acclimation in realistic field environments. This study aimed to (1) investigate the impact of FL on soybean morphology and photosynthetic parameters, (2) evaluate the reduction in carbon assimilation caused by FL, and (3) determine the response kinetics of gas exchange and chlorophyll (Chl) fluorescence parameters to FL, identifying factors responsible for decreased carbon gain under FL.

2. Materials and methods

2.1. Plant materials and experimental design

Experiments were conducted at the College of Agriculture, Sichuan Agricultural University, Chengdu, China. The experiments were carried out in a plant factory with a day/night temperature regime of 25°C/22°C and a photoperiod of 12 h light/12 h dark. The experiment used Guixia 7, a widely adopted genotype for intercropping studies. Soybean seeds were sown in a soil mixture of vermiculite and nutrient soil (Pindstrup Substrate, Denmark) at a 1:3 (v:v) ratio. The substrate was sterilized with carbendazim. After germination, seedlings were transferred to designated light treatments. Four light intensity treatments were applied (Fig. 1-A): HL at 1,200 μmol m^{-2} s^{-1}, medium-light (ML) at 500 μmol m^{-2} s^{-1}, LL at 150 μmol m^{-2} s^{-1}, and FL, alternating between 1,200 and 150 μmol m^{-2} s^{-1}. The height of the seedbed was adjusted during growth to maintain a 15 cm distance between the top of the canopy and the light source. The FL regime was controlled using a programmable system (VQ-VD-100, VANQ, Shenzhen, China). The cumulative daily light integral was equal for FL and ML treatments (Fig. 1-B).

2.2. Evaluation of leaf morphological characteristics and biomass

Four plants per treatment were randomly selected to measure individual leaf area. Images were captured using a Nikon D5600 camera (Nikon Inc., Tokyo, Japan), and leaf area was quantified using ImageJ software (National Institutes of Health, Bethesda, MD, USA). Aboveground parts and roots were separated, placed in paper bags, and blanched at 105°C for 1 h. Samples were then dried at 80°C to constant weight and weighed using an electronic balance. Specific leaf weight was calculated as the ratio of dry mass to leaf area.

2.3. Chl content

For Chl analysis, 0.1 g of fresh leaf tissue was extracted in 8 mL of 95% acetone for 24 h at 25°C in darkness.

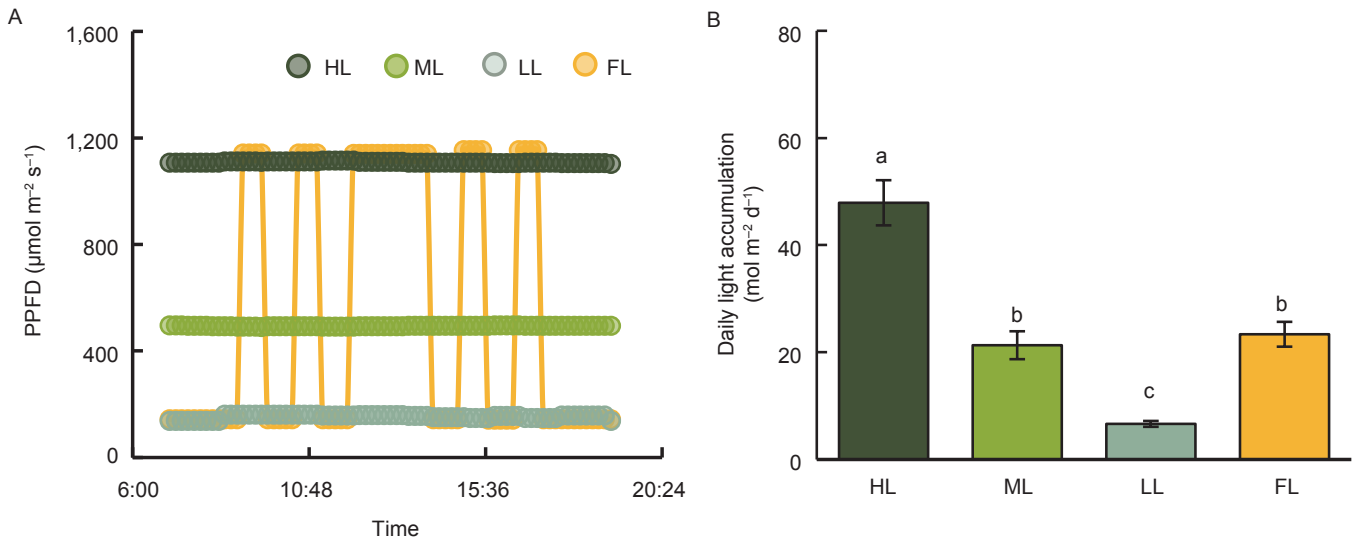


Fig. 1 Light environment in the experimental treatments. A, daily variations in light intensity. B, average daily light intensity. HL, high-light; ML, medium-light; LL, low-light; FL, fluctuating light. Data are represented as mean±SD (n=6). Different lowercase letters indicate statistically significant differences between different treatments at the P<0.05 level.

Absorbance was measured using a spectrophotometer (T80, Beijing, China) at 645 nm (Chl *b*) and 665 nm (Chl *a*). Concentrations were expressed in mg g^{-1} FW. The Chl *a*/Chl *b* ratio was calculated following established procedures (Tang *et al.* 2023).

2.4. Steady-state gas exchange measurements

Photosynthetic rates of soybean leaves were measured in a controlled environment chamber. Six fully expanded leaves per treatment were analyzed using the LI6400-02B chamber of a Li-Cor 6400 Portable Photosynthesis System (Li-Cor Inc., USA). Light intensity in the chamber was set to 1,200, 500, or 150 μmol m^{-2} s^{-1} to match growth conditions. Leaf-to-air vapor pressure deficit was maintained at 1.5–2.0 kPa, and CO_2 concentration was kept at 400 μmol mol^{-1} using a CO_2 mixer. Chamber temperature was held at 25°C. Once steady-state conditions were reached, net photosynthetic rate (P_n), stomatal conductance (G_s), intercellular CO_2 partial pressure (C_i), and transpiration rate (E) were recorded (Gao *et al.* 2023).

2.5. Stomatal traits

Following gas exchange measurements, 1 cm^2 leaf sections were collected from the top, middle, and bottom regions of each leaf. Tissue samples were fixed in formalin–acetic acid–alcohol (FAA) solution for 24 h. All sampling occurred at the same time of day. Tissues were decolorized in a graded ethanol series (50, 70, 85, 95, and 100%) for 30 min each, then soaked in 5% NaOH (w/v) for 2 d. After rinsing with distilled water, samples were treated with trichloroacetaldehyde hydrate until translucent. Finally, they were stained with 1% methylene blue, rinsed, mounted on slides, and imaged (Gao *et al.* 2023). Three images per leaf were captured using a TI-E inverted fluorescence microscope (Nikon Inc., Tokyo, Japan) at 10× and 30× magnification. ImageJ software was used to determine stomatal density. Stomatal size was calculated based on the length of the longest axis of each stoma (Wang *et al.* 2014).

2.6. Ultrastructure of leaf tissue

Leaf tissues were cut into 5 mm×5 mm pieces and fixed in 2.5% glutaraldehyde (v/v) at 4°C for 24 h. Fixed tissues were washed three times in PBS (10 min each). Sections were then immersed in 1% osmium tetroxide for 40 min, dehydrated through a graded alcohol series, infiltrated with Spurr resin (SPI Chem, West Chester, PA, USA), and polymerized at 65°C for 48 h. Ultrathin sections (50–60 nm) were stained with 2% uranyl acetate (Jiang *et al.* 2011) and examined using a scanning transmission electron microscope (Tecnai G2 Spirit Bio-TWIN) at ×15,000 and ×2,000 magnifications. Cell wall thickness (TCW) was measured at ×15,000. The surface area of chloroplasts exposed to intercellular space per unit leaf area (S_c) and mesophyll cell wall surface area per unit leaf area (S_m) were calculated as follows (Han *et al.* 2018):

$$S_m = \frac{F \times L_m}{L}$$

$$S_c = \frac{F \times L_c}{L}$$

As shown in Appendix A, cross-sectional width (L), total length of mesophyll cell wall exposed to intercellular air space (L_m), and total length of chloroplasts in contact with plasma membrane facing intercellular space (L_c) were measured from micrographs. F is the calibration coefficient. Values of F for palisade and spongy mesophyll were 1.470 and 1.14, respectively (Théroux-Rancourt *et al.* 2017). The palisade-to -spongy mesophyll ratio under different treatments was quantified separately and averaged to determine F values used in calculations.

2.7. Leaf anatomy

Leaf sections (0.5 cm×0.5 cm) were excised and fixed

in formaldehyde, acetic acid and ethanol (FAA) solution. Tissues were embedded in paraffin and sectioned at 10 μm using a microtome. Sections were stained with hematoxylin–eosin and sealed with neutral resin. Images were acquired using an Eclipse 80i microscope (Nikon Inc., Tokyo, Japan) with ACT-2U imaging software.

Leaf thickness (T_{leaf}) was determined by dividing the cross-sectional area by the width of the section in light microscope images (Appendix B), following methods described by Huang *et al.* (2022) and Gao *et al.* (2023):

$$T_{leaf}=\frac{\text{Area of cross section}}{\text{Width of cross section}}$$

Total mesophyll cross-sectional area and intercellular air space area were directly measured. The fraction of mesophyll volume occupied by intercellular air space (f_{IAS}) was calculated as (Hu *et al.* 2022):

$$f_{IAS}=\frac{\text{Area of intercellular air space}}{\text{Area of cross section}}$$

2.8. Light response curves

CO_2 concentration in the Li-6400 chamber was maintained at 400 μmol mol^{-1} using an injection system. An automated program applied a light gradient: 2,300, 1,700, 1,200, 900, 500, 300, 200, 150, 100, 50, 20, and 0 μmol m^{-2} s^{-1}. Initial chamber light was set to 2,300 μmol m^{-2} s^{-1}. After inserting the leaf, a 10–20 min acclimation period was allowed. Measurements were recorded once photosynthetic parameters stabilized. Data were fitted to a rectangular hyperbolic model to derive parameters such as A_{sat} and maximum apparent quantum yield (AQY) for each treatment (Herrmann *et al.* 2020). Six uniformly growing plants per treatment were selected.

2.9. CO_2 response curve

Prior to measurement, chamber CO_2 was maintained at 400 μmol mol^{-1}, and light intensity was set to saturating levels for each treatment. Leaves were acclimated for 10–20 min until parameters stabilized. CO_2 concentrations were generated by injection: 400, 300, 200, 150, 100, 50, 400, 400, 600, 800, 1,000, 1,200, 1,500, 1,800, and 2,000 μmol mol^{-1}. Parameters including CO_2 compensation point and saturation point were derived using a corrected rectangular hyperbola model (Greer 2015):

$$P_n(C_i)=\frac{\alpha V_{cmax} C_i}{\alpha C_i+V_{cmax}}-R_d$$

where α represents initial carboxylation efficiency (CE), and R_d is the photorespiration rate. Since dark respiration is negligible under light, CO_2 release approximates photorespiration. Maximum carboxylation rate (V_{cmax}) was estimated using the Farquhar-von Caemmerer-Berry model implemented in R_{studio} (Duursma 2015).

2.10. Mesophyll conductance and CO_2 concentration within chloroplasts

Mesophyll conductance (G_m) was calculated using the variable *J* method (Harley *et al.* 1992):

$$G_m=P_n/\left\{C_i-\frac{\Gamma^*[J_f+8(P_n+R_d)]}{J_f-4(A+R_d)}\right\}$$

$$C_c=C_j-\frac{P_n}{G_m}$$

where Γ^* is the CO_2 compensation point without respiration, R_d is daytime respiration, J_{max} is electron transport rate, and C_c is chloroplastic CO_2 concentration.

J_{max} was computed as:

$J_{max}=\Phi_{PSII}\cdot PPFD\cdot\alpha\cdot\beta$

α denotes leaf absorbance, β represents electron partitioning between PSI and PSII. Φ_{PSII} reflects actual photochemical efficiency of PSII, calculated as:

$$\Phi_{PSII}=\frac{(F'_m-F_s)}{F'_m}$$

Φ_{PSII} was measured using a LI-6400–40 chamber. Chamber CO_2 was maintained at 400 μmol mol^{-1} with a flow rate of 300 μmol s^{-1}. Temperature was held at (25±3)°C. PAR settings were 1,200, 500, and 150 μmol m^{-2} s^{-1}. Steady-state fluorescence (F_s) and maximum fluorescence (F'_m) were recorded after stabilization (Xiong *et al.* 2015).

Since R_d is light-dependent, it was directly measured by introducing 1% O_2 into the LI-6400 under conditions similar to ΦPSII measurements (Yin *et al.* 2011), rather than derived from curve fitting.

To estimate α and β, low-oxygen fluorescence response curves were measured. These parameters were derived from the slope of linear regression between P_n and photosynthetic photon flux density (PPFD)$\cdot\Phi_{PSII}$/4 (Yin and Struik 2009). Plants were dark-adapted in the LI-6400-40 chamber (flow rate: 300 μmol s^{-1}) for ≥30 min. Dark-adapted fluorescence parameters F_o and F_m were recorded. For low-O_2 measurements, 1% O_2 was introduced while maintaining CO_2 at 400 μmol mol^{-1} *via* injection. Flow rate was 300 μmol s^{-1}. R_d values were input based on prior measurements. An automated program applied the same light gradient as above. Gas exchange and Chl fluorescence data were recorded simultaneously upon stabilization.

T^* was calculated by fitting the Laisk method (Tomeo and Rosenthal 2017). Chamber temperature was (25±3)°C, flow rate 300 μmol s^{-1}. Low-CO_2 response curves were measured at PAR levels of 300, 235, 175, and 125 μmol m^{-2} s^{-1}, with CO_2 gradients of 90, 75, 50, and 40 μmol mol^{-1}. Each PPFD change required a 10–20 min adjustment. C_i^* and P_n were regressed linearly. The absolute slope gives C_i^*, and the average is denoted as T^*.

2.11. Calculation of carbon assimilation during photoinduction

Dynamic photosynthetic parameters under FL were measured using a Li-Cor 6400 infrared gas analyzer. Chamber CO_2 was maintained at 400 ppm, temperature at 25°C, vapor pressure deficit at (1.3±0.2) kPa, and flow rate at 500 μmol s^{-1}. An initial adaptation phase at 150 μmol m^{-2} s^{-1} was maintained until steady-state P_n and G_s were achieved. Light was then increased to 1,200 μmol m^{-2} s^{-1} for 30 min. Gas exchange data were logged every 10 s; Chl fluorescence every 2 min. Light was then returned to 150 μmol m^{-2} s^{-1}, and parameters recorded for another 30 min. Carbon gain and loss were calculated as:

Carbon gain=$A_t\cdot d_t$

Carbon loss=$A_t \cdot \Delta_t - A_t \cdot d_t$

2.12. Calculation of the response rate of photosynthetic parameters to light intensity changes

Time courses of five parameters — P_n, G_s, G_m, V_{cmax}, and J_{max} — were fitted to a Boltzmann sigmoid function:

$$f_{(t)} = X_{min} + \frac{X_{max} - X_{min}}{1 + \exp(T_{50} - t)/d_t}$$

where X_{min} and X_{max} are parameter minimum and maximum values; $d_t = (X_{max} - X_{min})/(4 \times \text{slope at inflection})$; T_{50} is the time to reach 50% of maximum after HL exposure. T_{90} was also derived to indicate time to 90% of maximum (Givnish 1988).

2.13. Statistical analysis

Data were organized and graphed using Microsoft Excel 2022. Statistical analyses were performed using SPSS 25.0. Differences among treatments were assessed using one-way ANOVA followed by Duncan's *post-hoc* test. After normality testing, Pearson correlation analysis was applied.

3. Result

3.1. Soybean plant morphology varies under different light intensity treatments

Soybean morphological traits varied significantly across light treatments (Fig. 2-A). FL treatment inhibited growth, reducing aboveground and root dry weights by 49.92 and 71.18%, respectively, compared to ML (Fig. 2-B). Leaf area, leaf thickness, and specific leaf weight decreased by 26.11, 22.32, and 39.41%, respectively (Fig. 2-C–E). FL also significantly reduced the Chl *a*/Chl *b* (Fig. 2-F). Compared to HL treatment, ML did not differ significantly in aboveground dry weight, but root dry weight was significantly lower. LL treatment caused substantial reductions in both aboveground and root biomass (Fig. 2-B). Leaf area declined by 39.27% under LL, whereas ML increased it by 40.84% (Fig. 2-C). ML and LL treatments resulted in significantly lower specific leaf weight and leaf thickness than HL (Fig. 2-D and E).

3.2. Variations in photosynthetic parameters under different light intensity treatments

Leaf photosynthesis contributes critically to biomass accumulation during seedling growth. Photosynthetic parameters were measured under various light intensities. A_{sat} decreased by 23.91% under ML and 59.05% under LL compared to HL (Fig. 3-B). No significant difference in A_{sat} was observed between ML and FL, suggesting FL minimally affects photosynthetic capacity. CE, reflecting performance under low CO_2, was significantly lower in ML and LL than HL (Appendix C), but not between FL and ML. AQY, indicating LL photosynthetic capacity, showed no significant differences among treatments. J_{max} did not differ between ML and FL, but V_{cmax} was significantly lower under FL than ML (Appendix C).

3.3. Variations in leaf gas exchange parameters under different light intensity treatments

P_n, G_m, and G_s under FL did not differ significantly from ML (Table 1). However, E under FL was 114.81% higher than

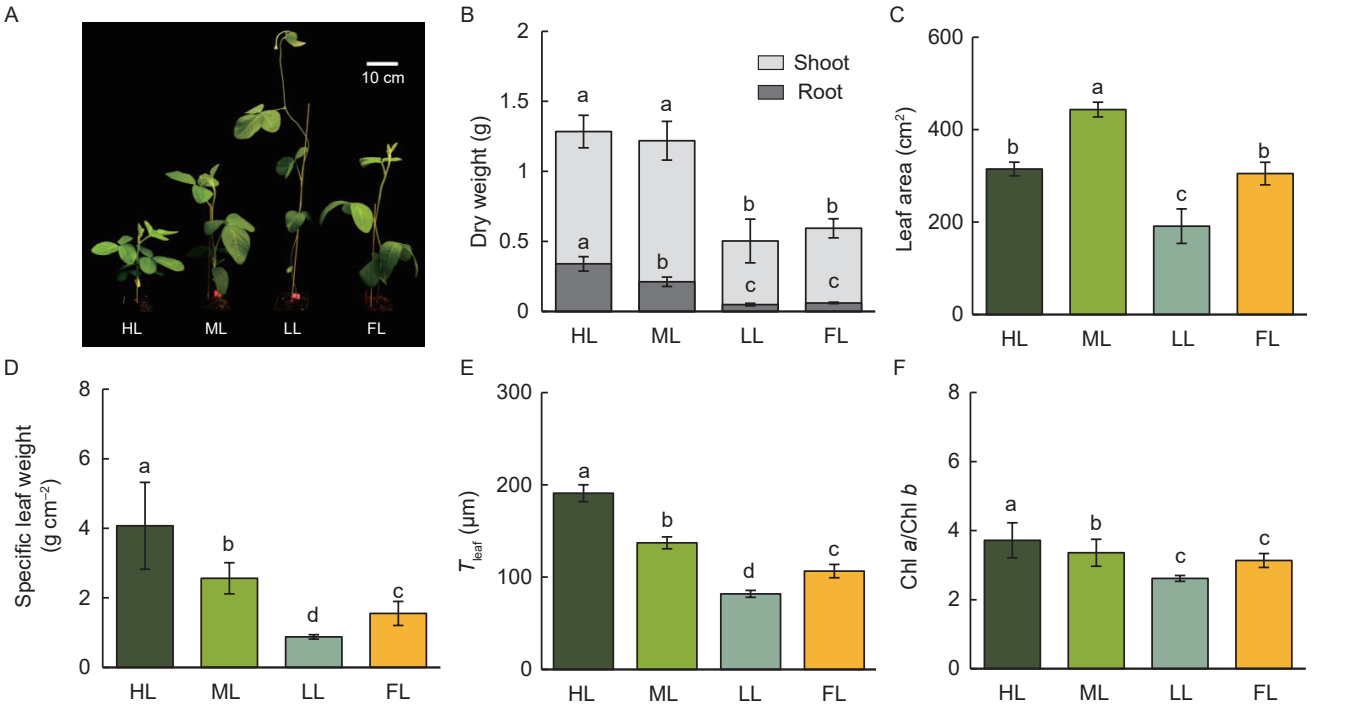


Fig. 2 Influence of varied growth light environments on soybean seedling growth. A, photographs of soybean plants in each treatment group. B, dry matter mass of shoots and roots. C, total leaf area of the whole plant. D, specific leaf weight. E, leaf thickness. F, chlorophyll (Chl) *a* to Chl *b* ratio. HL, high-light; ML, medium-light; LL, low-ight; FL, fluctuating light. T_{leaf}, leaf thickness, Chl *a*/Chl *b*, ratio of Chl *a* to Chl *b*. Bars mean SD (n=6). Different lowercase letters indicate statistically significant differences between different treatments at the P<0.05 level.

under ML. In contrast, gas exchange parameters in seedlings were sensitive to reduced light. P_n decreased significantly in ML and LL versus HL. G_s and G_m were reduced under ML and further under LL. C_i increased under LL compared to HL. No significant differences in C_c were observed among treatments. Transpiration decreased under LL, with E notably lower under LL than HL.

3.4. Stomatal morphological characteristics and structural limiting factors of G_m in response to different light intensity treatments

A correlation analysis revealed that reduced P_n under LL coincided with declines in G_m and G_s (Appendix D). To explore causes of reduced G_s, stomatal morphology was analyzed. Stomatal density decreased significantly under LL, but size remained unchanged. To assess structural constraints on G_m, leaf anatomy was examined. Light reduction did not increase TCW or f_{IAS}. However, S_m and S_c declined significantly with decreasing light (Appendix D).

3.5. Dynamic changes of leaf gas exchange and photosynthetic parameters under FL in soybean

After reaching steady-state photosynthesis under LL, leaves were exposed to 30 min of HL, followed by 30 min of LL Carbon assimilation under FL was quantified. FL caused carbon assimilation loss (Fig. 4), particularly during the induction phase. Dynamic changes in gas exchange and photosynthetic parameters are shown in Fig. 5. Upon transition to HL, P_n increased rapidly and stabilized. In contrast, G_s rose gradually, continuing beyond 1,000 s. The quantum efficiencies of CO_2 assimilation (ΦCO_2) and ΦPSII dropped quickly to minima and recovered slowly. When light surged from 150 to 1,200 μmol m^{-2} s^{-1}, P_n initially declined, then recovered.

Temporal responses during light induction were shown in Fig. 6-A and B. Time to reach 50% of maximum increased in the order: J_{max}, P_n, G_s, V_{cmax}. Response rates to 95% of maximum varied. J_{max} responded fastest; G_s was significantly slower. NPQ induced rapidly upon HL exposure but relaxed gradually when light decreased (Fig. 6-C).

A significant positive correlation existed between carbon assimilation loss during induction and time for G_s to reach 95% of maximum (Fig. 7-A). Similarly, post-irradiation carbon loss correlated positively with time for NPQ to relax to 95% (Fig. 7-B). A strong positive correlation was observed between P_n and G_s during induction (Fig. 7-C). During post-irradiation, NPQ showed a significant negative correlation with ΦCO_2 (R^2=0.96; Fig. 7-D).

4. Discussion

4.1. Soybean response to FL: Similarities to shade acclimation traits

FL negatively affected soybean growth, reducing whole-plant leaf area, specific leaf weight, and dry matter compared to steady light (Fig. 2-B–E). FL strongly inhibited root growth, with greater reduction in root dry weight than in

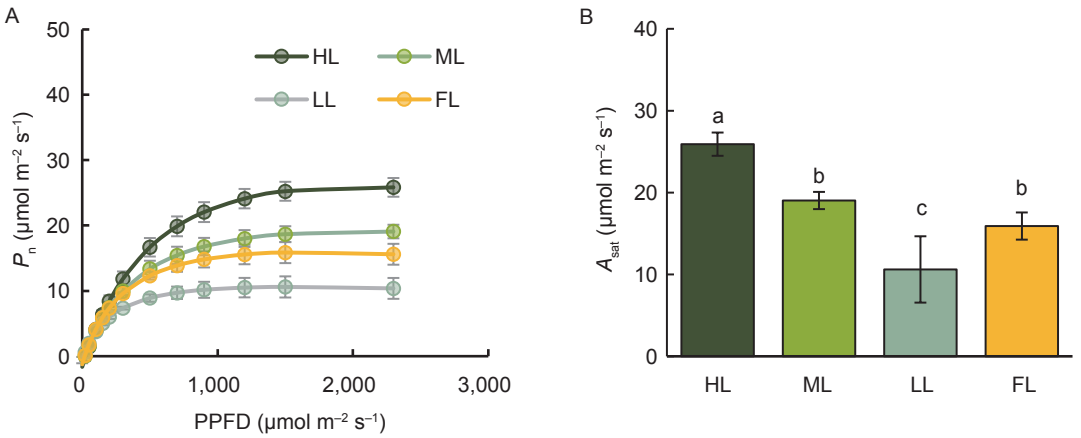


Fig. 3 Influence of diverse growth light environments on net photosynthetic light-response curves (P_n-PPFD) in soybean seedlings. A, leaf photosynthesis–light curves. B, the maximum photosynthetic rate. HH, high-light; ML, medium-light; LL, low-light; FL, fluctuating light. A_{sat}, the maximum photosynthetic rate. Bars mean SD (n=6). Different lowercase letters indicate statistically significant differences between different densities at the P<0.05 level.

Table 1 Variations in leaf gas exchange parameters under different light treatments[1)]

Treatment	P_n (μmol m^{-2} s^{-1})	G_s (mol m^{-2} s^{-1})	C_i (μmol mol^{-1})	G_m (mol m^{-2} s^{-1})	C_c (μmol mol^{-1})	E (mol m^{-2} s^{-1})
High-light	21.26±2.72 a	0.27±0.08 a	267.89±21.18 b	0.19±0.05 a	153.35±19.31 a	2.09±0.13 a
Medium-light	14.66±2.47 b	0.26±0.05 a	279.57±33.49 b	0.15±0.05 a	162.62±38.18 a	1.17±0.11 b
Low-light	3.71±0.76 c	0.02±0.009 b	301.09±17.20 a	0.03±0.02 b	143.44±30.09 a	1.33±0.33 b
Fluctuating-light	16.34±3.13 d	0.22±0.06 a	286.12±33.32 b	0.12±0.03 a	146.04±23.11 a	2.51±0.21 a

[1)] P_n, net assimilation rate; G_s, stomatal conductance; C_i, intercellular CO_2 concentration; G_m, mesophyll conductance; C_c, CO_2 concentration in the chloroplast stroma, E, transpiration rate.
Data are shown as mean±SD (n=6). Different letter means significant difference at P<0.05.

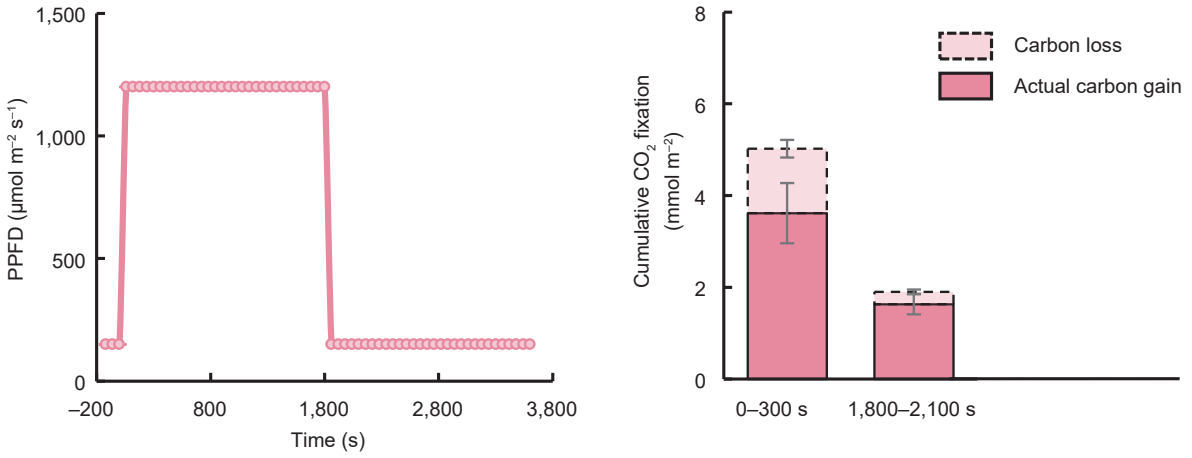


Fig. 4 Cumulative CO_2 fixation during the initial 5 min following photosynthesis induction and the subsequent 5 min after the post-irradiance stage. Differences between the solid and dashed lines represent the loss in photosynthetic carbon assimilation during light fluctuations.

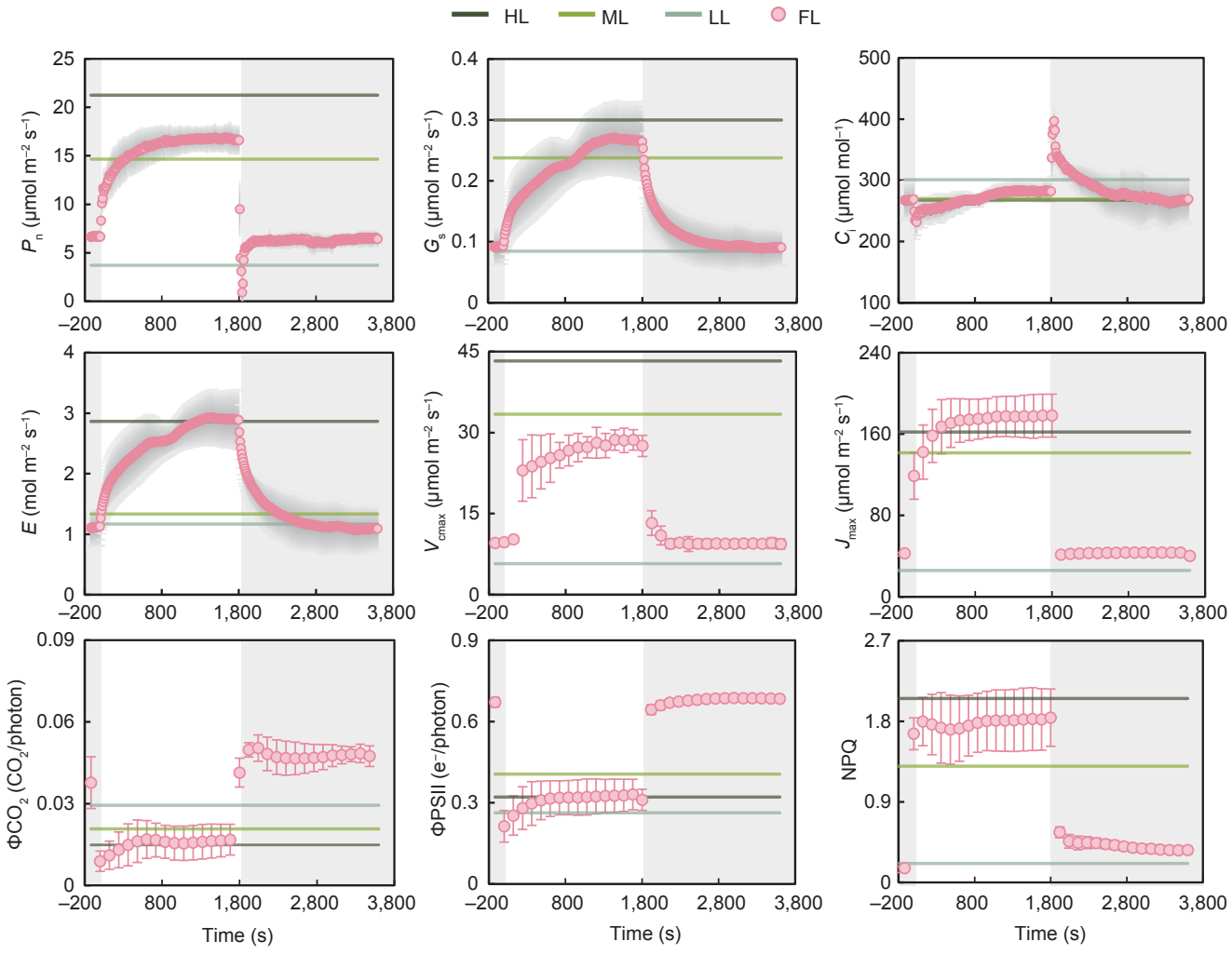


Fig. 5 Responses of photosynthetic gas exchange parameters and chlorophyll (Chl) *a* fluorescence parameters in soybean during alternating high- and low-light conditions. The gray boxes in each figure represent the periods of low-light, whereas the white boxes represent the periods of high light. P_n, net assimilation rate; G_s, stomatal conductance; C_i, intercellular CO_2 concentration; E, transpiration rate; V_{cmax}, maximum carboxylation rate of Rubisco; J_{max}, maximum electron transport rate; ΦCO_2, quantum efficiencies of CO_2 assimilation; ΦPSII, actual photochemical efficiency of photosystem II; NPQ, nonphotochemical quenching. Bars mean SD (n=6).

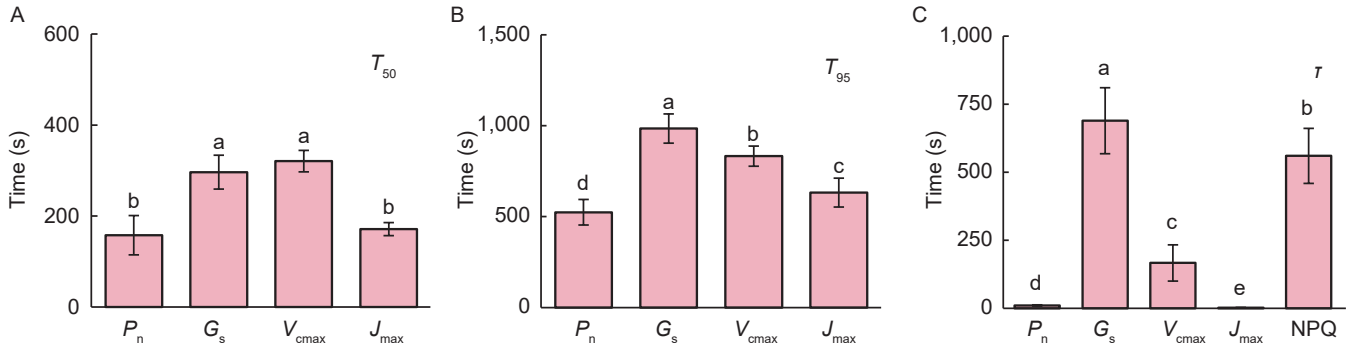


Fig. 6 Response speed of photosynthetic parameters to fluctuations in light intensity. The time it takes for photosynthetic parameters to reach 50% (T_{50}) (A) and 95% (T_{95}) (B) of their maximum values during photosynthetic induction. C, the time it takes for photosynthetic parameters to decrease by 95% during the transition from HL to LL (τ). P_n, net CO_2 assimilation rate; G_s, stomatal conductance; V_{cmax}, the maximum rate of RuBP carboxylation; J_{max}, the maximum rate of electron transport; NPQ, nonphotochemical quenching. Bars mean SD (n=6). Different lowercase letters indicate statistically significant differences between different groups at the P<0.05 level.

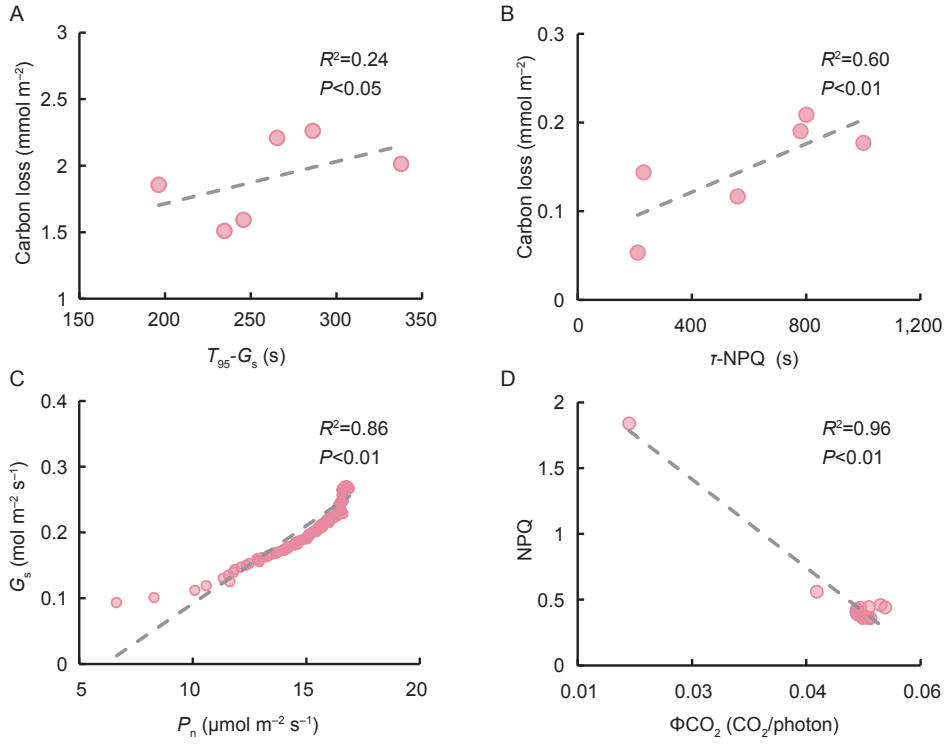


Fig. 7 Correlation analysis of photosynthetic parameters and carbon assimilation in fluctuating light. A, relationship between the loss in photosynthetic carbon assimilation and the time it takes for stomatal conductance to reach 95% of their maximum value (T_{95}-G_s) during photosynthetic induction. B, relationship between the loss in photosynthetic carbon assimilation and the time it takes for nonphotochemical quenching (NPQ) to decrease by 95% during the post-irradiation stage. C, relationship between stomatal conductance (G_s) and net assimilation rate (P_n) after changing from LL to HL. D, correlation analysis of NPQ and quantum efficiencies of CO_2 assimilation (ΦCO_2). The sample size employed in all correlation analyses was identical, n=6. R^2 represents the coefficient of determination, P<0.05 was considered significant, whereas P<0.01 was markedly significant.

aboveground biomass. This response varies by species: wheat and Amaranthus caudatus show reduced root/shoot ratios under FL, while Celosia argentea does not (Karpinski *et al.* 2013). The Chl *a*/Chl *b* was lower in FL-treated leaves than ML (Fig. 2-F), indicating relatively more light-harvesting complexes relative to reaction centers in PSII — a trait typical of shade-acclimated leaves (Albanese *et al.* 2018). Morales and Kaiser (2020) noted that plants under FL exhibit ~12% higher specific leaf area. In this study, specific leaf weight was significantly lower in FL-grown seedlings (Fig. 2-D), suggesting development of thinner, less dense leaves — a common shade-acclimation-like response (Evans and Poorter 2001).

Soybeans under FL exhibit traits resembling shade adaptation. This raises the question: Are these physiological changes due to acclimation to low-irradiance phases during

FL? While FL includes LL periods absent in ML, unlike morphological changes, FL did not induce shade-type alterations in CO_2 assimilation (Table 1). Photosynthetic capacity, indicated by A_{sat}, was unaffected by FL (Fig. 3-B). Under LL, coordinated changes in stomatal and anatomical traits reduced carbon availability, lowering photosynthetic capacity (Appendix D). Morales and Kaiser (2020) similarly reported minimal FL impact on photosynthetic capacity. These findings suggest FL acclimation is distinct from LL acclimation. Cumulative daily light was equal for FL and ML, ruling out light deficiency as a cause of "shade-like" morphology. Tomimatsu and Tang (2016) showed that herbaceous plants assimilate less carbon under FL at low CO_2, but elevated CO_2 enhances carbon gain. Thus, FL-induced growth inhibition in soybean likely stems from reduced carbon assimilation, not light deficiency.

4.2. Carbon assimilation reduction: A delayed photosynthesis response rather than altered photosynthetic capacity in FL

The reduction in carbon assimilation was not due to diminished photosynthetic capacity, but to delayed photosynthetic responses under FL. Stomatal opening was notably slower than photosynthetic induction. Time for G_s to reach 95% of maximum exceeded that for other parameters. Xiong *et al.* (2021) found rice stomatal conductance matches photosynthesis rate, possibly due to dumbbell-shaped stomata requiring less osmotic change (Nunes *et al.* 2020), enabling faster response than soybean's kidney-shaped stomata. Light-induced stomatal movement regulates carbon assimilation and water use efficiency (Deans *et al.* 2019). Typically, stomatal response lags behind photosynthesis (Eyland *et al.* 2021). Here, G_s continued rising after P_n stabilized (~800 s), indicating desynchronization. This mismatch may reduce water use efficiency. Lawson and Blatt (2014) modeled that synchronizing stomatal and photosynthetic responses could improve internal water use efficiency by >20%. Therefore, enhancing coordination under FL is crucial for water conservation, drought resilience, and future yield improvement.

FL led to reduced photosynthetic carbon assimilation in soybean, particularly during the photosynthetic induction phase (Fig. 4). What factors constrain carbon assimilation in soybean? The relative significance of stomatal diffusion and biochemical limitations during photosynthetic induction varies notably among plant species. In rice, stomatal regulation exerts minimal influence during photosynthetic induction, where the primary constraints are biochemical processes associated with Rubisco carboxylation (Acevedo Siaca *et al.* 2020; Acevedo-Siaca *et al.* 2021). Sakoda *et al.* (2021) demonstrated that under FL conditions, stomatal dynamics significantly affect photosynthetic performance. In *Arabidopsis thaliana*, *Manihot esculenta*, and *Nicotiana tabacum*, stomatal opening plays a pivotal role in limiting photosynthetic induction under FL (De Souza *et al.* 2020; Sakoda *et al.* 2021). In soybean, our study indicates that the rate of stomatal opening is a key constraint. Soleh *et al.* (2016) support this interpretation, reporting that stomatal limitation progressively increases during induction in soybean. However, they suggest that the rate of Rubisco activation is the primary factor underlying genotypic differences in induction responses. Following abrupt increases in irradiance, J_{max} increased rapidly (Fig. 5), with its activation kinetics exceeding those of P_n (Fig. 6-B and C). This indicates that limitations in (2014) photosynthetic electron transport had negligible effects on P_n during induction.

A significant positive correlation was observed between the reduction in carbon assimilation during photosynthetic induction and the time required for stomatal conductance to reach 95% of its maximum (Fig. 7-A). Additionally, a strong positive correlation existed between G_s and P_n (Fig. 7-C). These findings imply that accelerating stomatal opening could enhance photosynthetic induction in soybean. Such an improvement may serve as a viable breeding target to increase whole-plant carbon gain and dry matter production under field conditions. Our study did not assess the potential inhibitory effect of leaf internal conductance to CO_2 diffusion in dynamic light environments. Previous studies suggest that G_m adjusts rapidly to changes in light intensity, thereby exerting minimal influence on P_n. However, recent evidence highlights a substantial limitation imposed by G_m during photosynthetic induction. This discrepancy arises because the variable J method, commonly used in steady-state measurements, is unsuitable for estimating G_m under dynamic conditions. In contrast, online carbon isotope discrimination methods, such as those employed by Liu *et al.* (2022), measure differential utilization rates of $^{12}CO_2$ and $^{13}CO_2$ during diffusion or biochemical reactions, enabling more accurate G_m estimation in FL.

The relaxation rate of NPQ is slower than its induction rate, potentially causing unnecessary reductions in CO_2 fixation under variable light (De Souza *et al.* 2022). Our results support this hypothesis. The time required for a 95% decline in NPQ substantially exceeded that for recovery (Fig. 7-C). Upon transitioning to LL conditions, ΦCO_2 gradually increased (Fig. 5), showing a significant negative correlation with NPQ (Fig. 7-D). This suggests that excitation energy available for CO_2 assimilation was dissipated as heat *via* sustained NPQ, resulting in a transient decrease in the photosynthetic quantum yield of CO_2 fixation after HL exposure. The extent of post-irradiance reduction in carbon assimilation showed a strong positive correlation with the duration of NPQ relaxation (Fig. 7-C). Therefore, NPQ may increasingly limit carbon assimilation in field environments due to frequent light fluctuations caused by cloud cover and wind-driven canopy movement (Fig. 8).

5. Conclusion

FL reduces soybean dry matter accumulation, leaf thickness, specific leaf weight, and the Chl *a*/Chl *b* levels. The inhibitory effect of FL on soybean growth stems from reduced carbon assimilation, not from diminished photosynthetic capacity, but rather from delayed responsiveness to changing light. During transitions from low to high light, slow stomatal opening restricts CO_2 supply, thereby limiting photosynthesis. Upon return to LL, delayed relaxation of photoprotective mechanisms impairs light use efficiency.

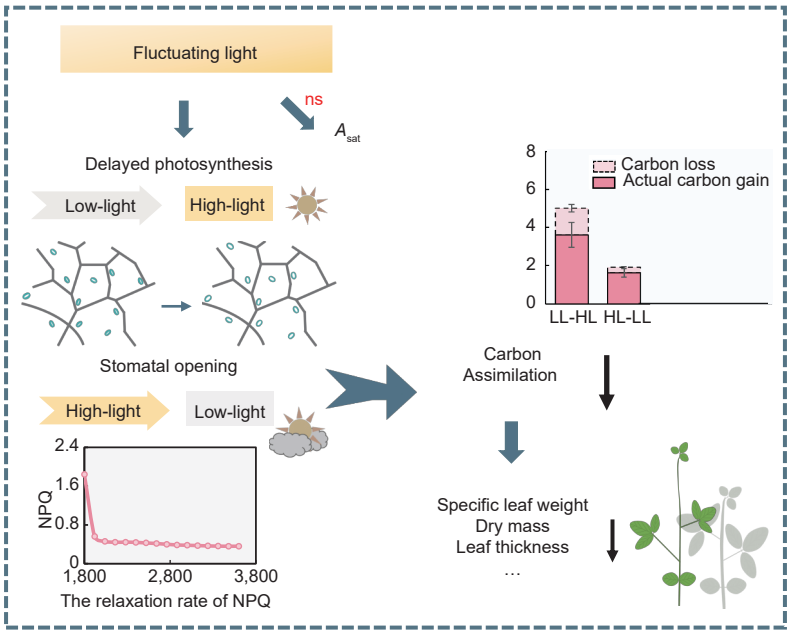


Fig. 8 Schematic of the effects of changes in carbon dioxide diffusion on soybean photosynthesis induced by fluctuating light. A_{sat}, the maximum photosynthetic rate; NPQ, nonphotochemical quenching; HL, high-light; LL, low-light. ns, not significant; ↓, decrease.

Acknowledgements

This research was supported by the National Key Research and Development Program of China (2023YFF1001504), the National Natural Science Foundation of China (32071963), the National Key Research and Development Program of China (2022YFD2300902), the Guangxi Key Research and Development Program of China (GuikeAB23026107), and the Chengdu Science and Technology Project, China (2023-YF08-00003-SN).

Declaration of competing interest

The authors declare that they have no conflict of interest.

Declaration of generative AI and AI-assisted technologies in the writing process

The authors declare that they did not use AI in the preparation and writing of this manuscript.

Appendices associated with this paper are available at https://doi.org/10.1016/j.jia.2024.07.032

References

Acevedo S L G, Coe R, Wang Y, Kromdijk J, Quick W P, Long S P. 2020. Variation in photosynthetic induction between rice accessions and its potential for improving productivity. *New Phytologist*, **227**, 1097–1108.

Acevedo S L G, Coe R, Quick W P, Long S P. 2021. Variation between rice accessions in photosynthetic induction in flag leaves and underlying mechanisms. *Journal of Experimental Botany*, **72**, 1282–1294.

Albanese P, Manfredi M, Re A, Marengo E, Saracco G, Pagliano C. 2018. Thylakoid proteome modulation in pea plants grown at different irradiances: quantitative proteomic profiling in a non-model organism aided by transcriptomic data integration. *Plant Journal*, **96**, 786–800.

Bassi R, Dall'Osto L. 2021. Dissipation of light energy absorbed in excess: the molecular mechanisms. *Annual Review of Plant Biology*, **72**, 47–76.

Blom T J, Zheng Y. 2009. The response of plant growth and leaf gas exchange to the speed of lamp movement in a greenhouse. *Scientia Horticulturae*, **119**, 188–192.

Deans R M, Brodribb T J, Busch F A, Farquhar G D. 2019. Plant water-use strategy mediates stomatal effects on the light induction of photosynthesis. *New Phytologist*, **222**, 382–395.

Duursma R A. 2015. Plantecophys — An R package for analysing and modelling leaf gas exchange data. *PLoS ONE*, **10**, e0143346.

Evans J R, Poorter H. 2001. Photosynthetic acclimation of plants to growth irradiance: the relative importance of specific leaf area and nitrogen partitioning in maximizing carbon gain. *Plant Cell and Environment*, **8**, 755–767.

Eyland D, van Wesemael J, Lawson T, Carpentier S. 2021. The impact of slow stomatal kinetics on photosynthesis and water use efficiency under fluctuating light. *Plant Physiology*, **186**, 998–1012.

Gao J, Chen J, Lei Y, Wang Q, Zou J, Ning Z, Tan X, Yang F, Yang W. 2023. Functional consequences of light intensity on soybean leaf hydraulic conductance: coordinated variations in leaf venation architecture and mesophyll structure. *Environmental and Experimental Botany*, **210**, 105301.

Garcia-Molina A, Leister D. 2020. Accelerated relaxation of photoprotection impairs biomass accumulation in arabidopsis. *Nature Plants*, **6**, 9–12.

Givnish T J. 1988. Adaptation to sun and shade: A whole-plant perspective. *Functional Plant Biology*, **2**, 63–92.

Greer D H. 2015. Seasonal changes in the photosynthetic response to CO_2 and temperature in apple (*Malus domestica* cv. 'red gala') leaves during a growing season with a high temperature event. *Functional Plant Biology*, **42**, 309–324.

Han J, Lei Z, Zhang Y, Yi X, Zhang W, Zhang Y. 2018. Drought-introduced variability of mesophyll conductance in gossypium and its relationship with leaf anatomy. *Physiologia Plantarum*, **166**, 873–887.

Harley P C, Loreto F, Di Marco G, Sharkey T D. 1992. Theoretical considerations when estimating the mesophyll conductance to CO_2 flux by analysis of the response of photosynthesis to CO_2. *Plant Physiology*, **98**, 1429–1436.

Herrmann H A, Schwartz J M, Johnson G N. 2020. From empirical to theoretical models of light response curves — linking photosynthetic and metabolic acclimation. *Photosynthesis Research*, **145**, 5–14.

Hu W, Lu Z, Gu H, Ye X, Li X, Cong R, Ren T, Lu J. 2022. Potassium

availability influences the mesophyll structure to coordinate the conductance of CO_2 and H_2O during leaf expansion. *Plant Cell and Environment*, **45**, 2987–3000.
Huang G, Shu Y, Peng S, Li Y. 2022. Leaf photosynthesis is positively correlated with xylem and phloem areas in leaf veins in rice (*Oryza sativa*) plants. *Annals of Botany*, **129**, 619–631.
Huber M, Nieuwendijk N M, Pantazopoulou C K, Pierik R. 2021. Light signalling shapes plant-plant interactions in dense canopies. *Plant Cell and Environment*, **44**, 1014–1029.
Jiang C, Wang X, Gao H, Shi L, Chow W S. 2011. Systemic regulation of leaf anatomical structure, photosynthetic performance, and high-light tolerance in sorghum. *Plant Physiology*, **155**, 1416–1424.
Kaiser E, Morales A, Harbinson J, Heuvelink E, Marcelis L. 2020. High stomatal conductance in the tomato flacca mutant allows for faster photosynthetic induction. *Frontiers in Plant Science*, **11**, 1317.
Karpinski S, Szechynska-Hebda M, Wituszynska W, Burdiak P. 2013. Light acclimation, retrograde signalling, cell death and immune defences in plants. *Plant Cell and Environment*, **36**, 736–744.
Kimura H, Hashimoto-Sugimoto M, Iba K, Terashima I, Yamori W. 2020. Improved stomatal opening enhances photosynthetic rate and biomass production in fluctuating light. *Journal of Experimental Botany*, **71**, 2339–2350.
Kromdijk J, Glowacka K, Leonelli L, Gabilly S T, Iwai M, Niyogi K K, Long S P. 2016. Improving photosynthesis and crop productivity by accelerating recovery from photoprotection. *Science*, **354**, 857–861.
Lawson T, Blatt M R. 2014. Stomatal size, speed, and responsiveness impact on photosynthesis and water use efficiency. *Plant Physiology*, **164**, 1556–1570.
Lehretz G G, Schneider A, Leister D, Sonnewald U. 2022. High non-photochemical quenching of vpz transgenic potato plants limits CO_2 assimilation under high light conditions and reduces tuber yield under fluctuating light. *Journal of Integrative Plant Biology*, **64**, 1821–1832.
Liu T, Barbour M M, Yu D, Rao S, Song X. 2022. Mesophyll conductance exerts a significant limitation on photosynthesis during light induction. *New Phytologist*, **233**, 360–372.
Matsubara S. 2018. Growing plants in fluctuating environments: why bother? *Journal of Experimental Botany*, **69**, 4651–4654.
Matthews J, Vialet-Chabrand S, Lawson T. 2018. Acclimation to fluctuating light impacts the rapidity of response and diurnal rhythm of stomatal conductance. *Plant Physiology*, **176**, 1939–1951.
Mcausland L, Vialet-Chabrand S, Davey P, Baker N R, Brendel O, Lawson T. 2016. Effects of kinetics of light-induced stomatal responses on photosynthesis and water-use efficiency. *New Phytologist*, **211**, 1209–1220.
Morales A, Kaiser E. 2020. Photosynthetic acclimation to fluctuating irradiance in plants. *Frontiers in Plant Science*, **11**, 268.
Nunes T, Zhang D, Raissig M T. 2020. Form, development and function of grass stomata. *Plant Journal*, **101**, 780–799.
Pao Y C, Stutzel H, Chen T W. 2019. A mechanistic view of the reduction in photosynthetic protein abundance under diurnal light fluctuation. *Journal of Experimental Botany*, **70**, 3705–3708.
Pignon C P, Jaiswal D, Mcgrath J M, Long S P. 2017. Loss of photosynthetic efficiency in the shade. An achilles heel for the dense modern stands of our most productive C_4 crops? *Journal of Experimental Botany*, **68**, 335–345.
Sakoda K, Yamori W, Groszmann M, Evans J R. 2021. Stomatal, mesophyll conductance, and biochemical limitations to photosynthesis during induction. *Plant Physiology*, **185**, 146–160.
Soleh M A, Tanaka Y, Kim S Y, Huber S C, Sakoda K, Shiraiwa T. 2017. Identification of large variation in the photosynthetic induction response among 37 soybean [*Glycine max* (L.) Merr.] genotypes that is not correlated with steady-state photosynthetic capacity. *Photosynthesis Research*, **131**, 305–315.
Soleh M A, Tanaka Y, Nomoto Y, Iwahashi Y, Nakashima K, Fukuda Y, Long S P, Shiraiwa T. 2016. Factors underlying genotypic differences in the induction of photosynthesis in soybean [*Glycine max* (L.) Merr.]. *Plant Cell and Environment*, **39**, 685–693.
De Souza A P, Burgess S J, Doran L, Hansen J, Manukyan L, Maryn N, Gotarkar D, Leonelli L, Niyogi K K, Long S P. 2022. Soybean photosynthesis and crop yield are improved by accelerating recovery from photoprotection. *Science*, **377**, 851–854.
De Souza A P, Wang Y, Orr D J, Carmo-Silva E, Long S P. 2020. Photosynthesis across african cassava germplasm is limited by rubisco and mesophyll conductance at steady state, but by stomatal conductance in fluctuating light. *New Phytologist*, **225**, 2498–2512.
Tang C, Luo M, Zhang S, Jia G, Tang S, Jia Y, Zhi H, Diao X. 2023. Variations in chlorophyll content, stomatal conductance, and photosynthesis in setaria ems mutants. *Journal of Integrative Agriculture*, **22**, 1618–1630.
Taylor S H, Long S P. 2017. Slow induction of photosynthesis on shade to sun transitions in wheat may cost at least 21% of productivity. *Philosophical Transactions of the Royal Society B-Biological Sciences*, **372**, 20160543.
Théroux-Rancourt G, Earles J M, Gilbert M E, Zwieniecki M A, Boyce C K, Mcelrone A J, Brodersen C R. 2017. The bias of a two-dimensional view: comparing two-dimensional and three-dimensional mesophyll surface area estimates using noninvasive imaging. *The New Phytologist*, **215**, 1609–1622.
Tomeo N J, Rosenthal D M. 2017. Variable mesophyll conductance among soybean cultivars sets a tradeoff between photosynthesis and water-use-efficiency. *Plant Physiology*, **174**, 241–257.
Tomimatsu H, Tang Y. 2016. Effects of high CO_2 levels on dynamic photosynthesis: carbon gain, mechanisms, and environmental interactions. *Journal of Plant Research*, **129**, 365–377.
Vialet-Chabrand S, Matthews J S, Simkin A J, Raines C A, Lawson T. 2017. Importance of fluctuations in light on plant photosynthetic acclimation. *Plant Physiology*, **173**, 2163–2179.
Wang Y, Burgess S J, de Becker E M, Long S P. 2020. Photosynthesis in the fleeting shadows: an overlooked opportunity for increasing crop productivity? *Plant Journal*, **101**, 874–884.
Wang Y, Noguchi K, Ono N, Inoue S, Terashima I, Kinoshita T. 2014. Overexpression of plasma membrane H^+-atpase in guard cells promotes light-induced stomatal opening and enhances plant growth. *Proceedings of the National Academy of Sciences of the United States of America*, **111**, 533–538.
Wu H Y, Qiao M Y, Zhang Y J, Kang W J, Ma Q H, Gao H Y, Zhang W F, Jiang C D. 2023. Photosynthetic mechanism of maize yield under fluctuating light environments in the field. *Plant Physiology*, **191**, 957–973.
Wu Y, Wang E, Gong W, Xu L, Zhao Z, Di He, Yang F, Wang X, Yong T, Liu J, Pu T, Yan Y, Yang W. 2023. Soybean yield variations and the potential of intercropping to increase production in china. *Field Crops Research*, **291**, 108771.
Xiong D, Liu X, Liu L, Douthe C, Li Y, Peng S, Huang J. 2015. Rapid responses of mesophyll conductance to changes of CO_2 concentration, temperature and irradiance are affected by N supplements in rice. *Plant, Cell & Environment*, **38**, 2541–2550.
Xiong Z, Dun Z, Wang Y, Yang D, Xiong D, Cui K, Peng S, Huang J. 2021. Effect of stomatal morphology on leaf photosynthetic induction under fluctuating light in rice. *Frontiers in Plant Science*, **12**, 754790.
Yamori W, Kusumi K, Iba K, Terashima I. 2020. Increased stomatal conductance induces rapid changes to photosynthetic rate in response to naturally fluctuating light conditions in rice. *Plant, Cell & Environment,* **43**, 1230–1240.
Yao X, Zhou H, Zhu Q, Li C, Zhang H, Wu J J, Xie F. 2017. Photosynthetic response of soybean leaf to wide light-fluctuation in maize–soybean intercropping system. *Frontiers in Plant Science*, **8**, 1695.
Yin X, Struik P C. 2009. Theoretical reconsiderations when estimating the mesophyll conductance to CO_2 diffusion in leaves of C_3 plants by analysis of combined gas exchange and chlorophyll fluorescence measurements. *Plant Cell and Environment*, **32**, 1513–1524.
Yin X, Sun Z, Struik P C, Gu J. 2011. Evaluating a new method to estimate the rate of leaf respiration in the light by analysis of combined gas exchange and chlorophyll fluorescence measurements. *Journal of Experimental Botany*, **62**, 3489–3499.
Zhang Y, Kaiser E, Marcelis L, Yang Q, Li T. 2020. Salt stress and fluctuating light have separate effects on photosynthetic acclimation, but interactively affect biomass. *Plant Cell and Environment*, **43**, 2192–2206.
Zheng B, Li Y T, Wu Q P, Zhao W, Ren T H, Zhang X H, Li G, Ning T Y, Zhang Z S. 2023. Maize (*Zea mays* L.) planted at higher density utilizes dynamic light more efficiently. *Plant Cell and Environment*, **46**, 3305–3322.

Executive Editor-in-Chief Shaokun Li
Managing Editor Ning Wang